

*Supplementary data*

**Interfacial Assembled Preparation of Porous Carbon Composites for  
Selective CO<sub>2</sub> Capture at Elevated Temperatures**

*Li-Ping Guo, Wen-Cui Li, Bin Qiu, Zhan-Xin Ren, Jie Du, An-Hui Lu\**

State Key Laboratory of Fine Chemicals, School of Chemical Engineering, Dalian  
University of Technology, Dalian 116024, P. R. China

\*E-mail: anhuilu@dlut.edu.cn

**Experimental data**

**Chemicals**

Chemicals	CAS number	Purity	Supplier
Resorcinol	108-46-3	≥ 99.5 %	Sinopharm Chemical Reagent Co., Ltd.
Ammonia solution	1336-21-6	25-28 wt %	
Formalin	50-00-0	37-40 wt %	
All chemicals were used as received without further purification.			

The Laponite platelets are circular and 25-35 nm in diameter with a thickness of approximately 1 nm and a density of 2570 kg/m<sup>3</sup>. The Laponite is composed of a two-layer silica tetrahedron and a single-layer magnesium octahedron. Chemical formula is Na<sub>0.7</sub>[(Li<sub>0.3</sub>Mg<sub>5.5</sub>Si<sub>8</sub>)O<sub>20</sub>(OH)<sub>4</sub>]. Water molecules, Na ions, and small amounts of Li ions reside in the interlayer gaps of Laponite.<sup>S1</sup> The Laponite has an overall negative charge on the surface with positively charged edges. The negative charge on the surface of the Laponite is stabilized by positively charged sodium (Na<sup>+</sup>) ions adsorbed on the surface of the Laponite. Laponite is selected owing to its high interlayer exchange-ability that allows the interlayer spacing to be readily controlled, as well as

its nanoscale particle size, which is suitable for hierarchical structure fabrication. Specifically, pre-loaded and molecular-level dispersion of resorcinol molecules on both surfaces of exfoliated Laponite nanoplates can substantially bridge the two sides, in parallel with uniform nucleation and in situ co-polymerization with the reactants through hydrogen bonding and electrostatic interactions. As a consequence, resorcinol-formaldehyde can feasibly copolymerize in the interfaces of the Laponite nanoplates, ensuring a smooth and uniform growth of the carbon precursor on both surfaces of a Laponite nanoplate, thus to form 3D assemblies.

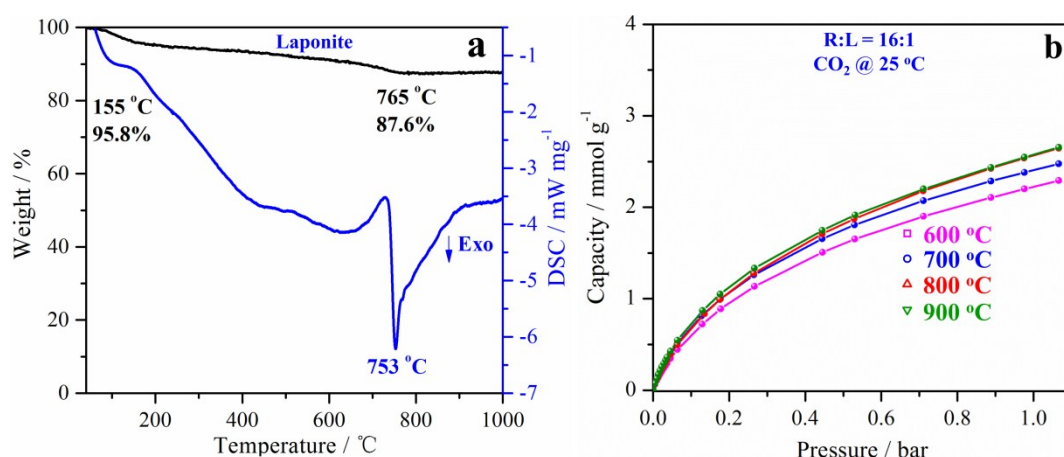


**Figure S1.** (a) TG and DSC analysis of the Laponite. (b) CO<sub>2</sub> adsorption isotherms of porous carbons prepared from composite polymer (R:L = 16:1), carbonized at different temperature (600, 700, 800 and 900 °C).

TG analysis was conducted to investigate the thermal stability of Laponite (Figure S1a). The small mass loss (4.2 wt%) below 155 °C is due to the evaporation of water that survived the drying process. The exothermic peak (753 °C) as shown by DSC profile is correspond to dehydroxylation peak.<sup>S2S3</sup> Notably, this TG curve shows a high residual weight (87.6 % at 1000 °C), clearly suggesting a relatively excellent

thermal stability of Laponite.

The CO<sub>2</sub> adsorption isotherms for porous carbon composites prepared *via* 2 h pyrolysis at various temperatures (600-900 °C) are shown in Figure S1b. As the pyrolysis temperature increases, there is a CO<sub>2</sub> adsorption capacity increasing to a maximum (2.6 mmol/g, 1.1 bar) and then it is unchanged at higher pyrolysis temperature. Therefore, 800 °C is set as the optimum pyrolysis temperature.

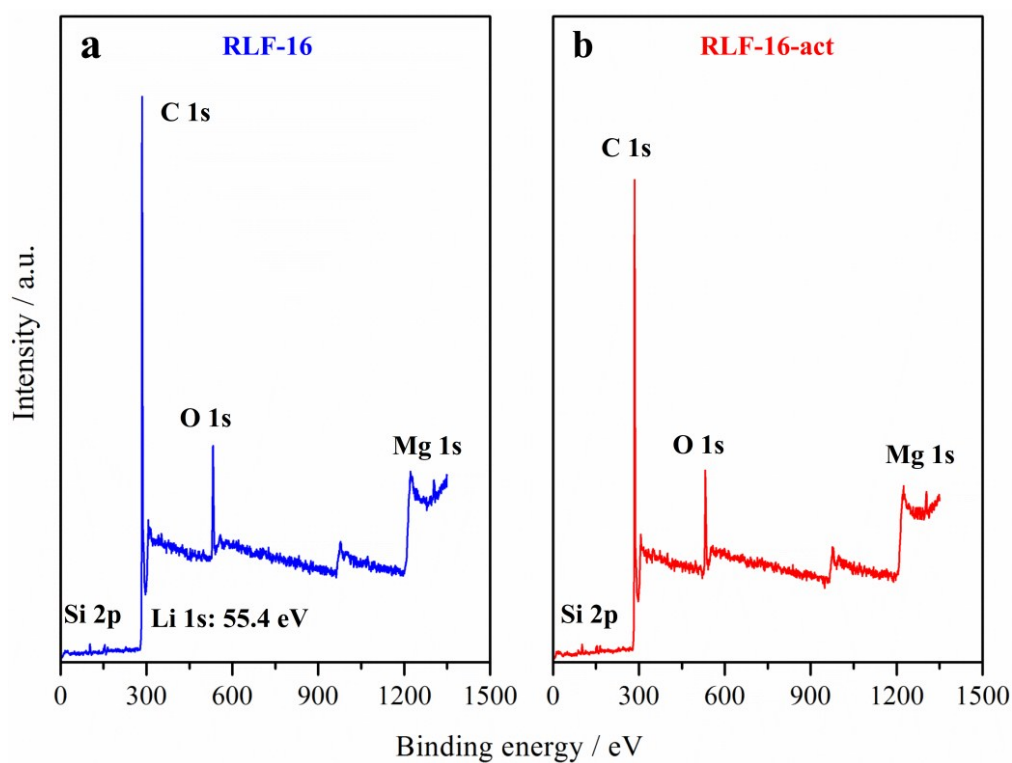


**Figure S2.** XPS survey spectra of (a) RLF-16 and (b) RLF-16-act.

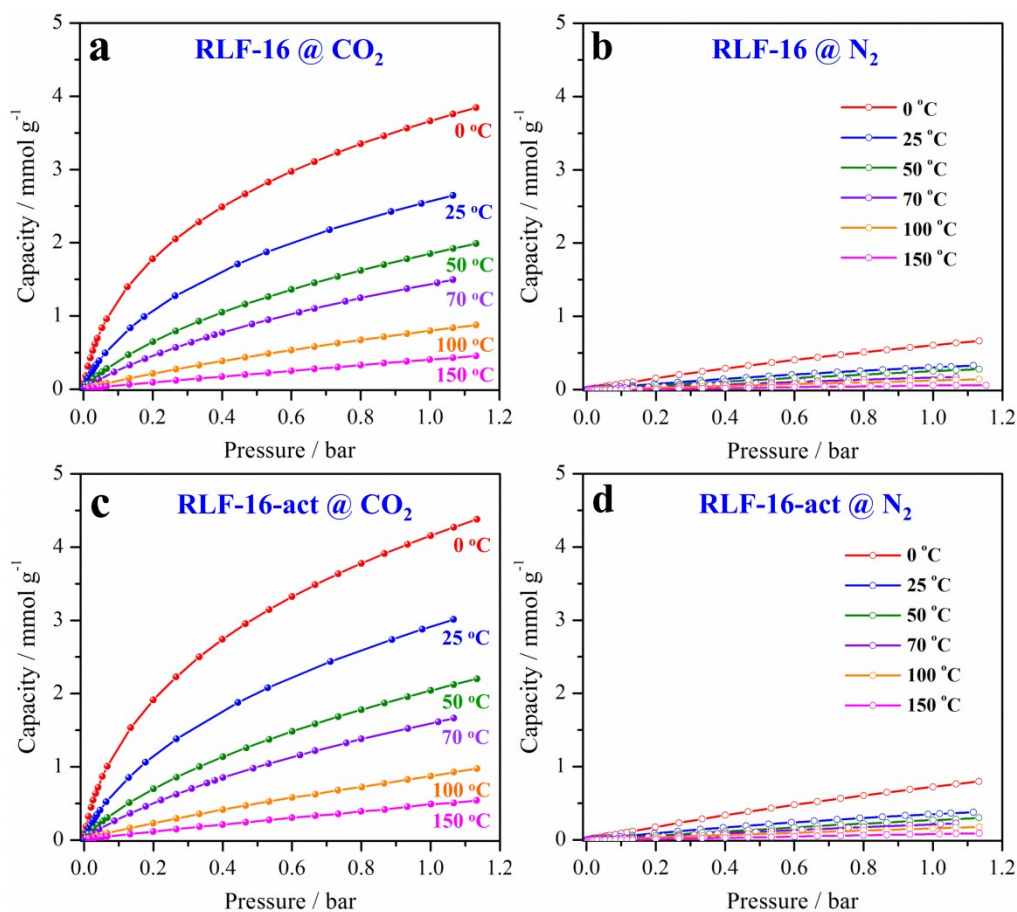


**Figure S3.** CO<sub>2</sub> adsorption isotherms as temperature function of (a) RLF-16, (c) RLF-16-act at 0, 25, 50, 70, 100 and 150 °C. N<sub>2</sub> adsorption isotherms of (b) RLF-16; (d) RLF-16-act at 0, 25, 50, 70, 100 and 150 °C.

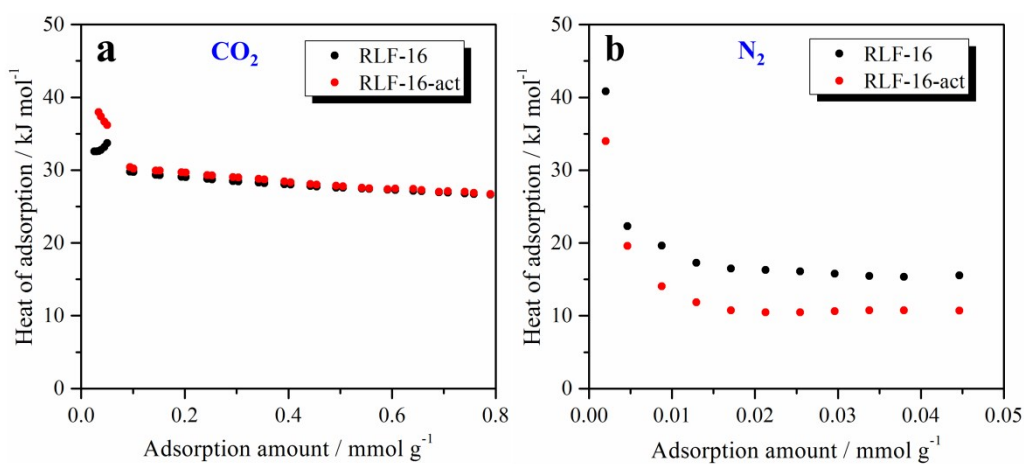


**Figure S4.** Isothermic heat of adsorption at varied adsorbed amounts of CO<sub>2</sub> (a) and N<sub>2</sub> (b) of RLF-16 and RLF-16-act at 1 bar.

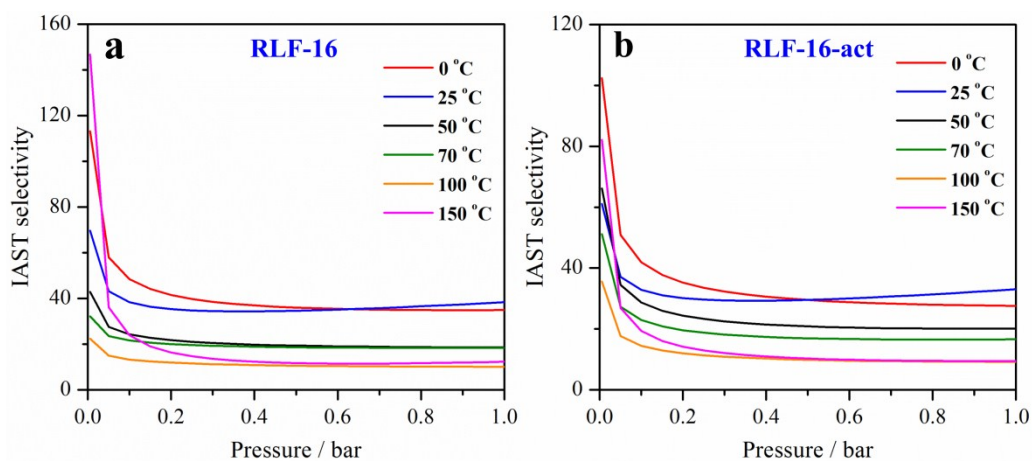


**Figure S5.** The IAST selectivities of RLF-16 and RLF-16-act for the CO<sub>2</sub>/N<sub>2</sub> (15/85 v/v) mixture.

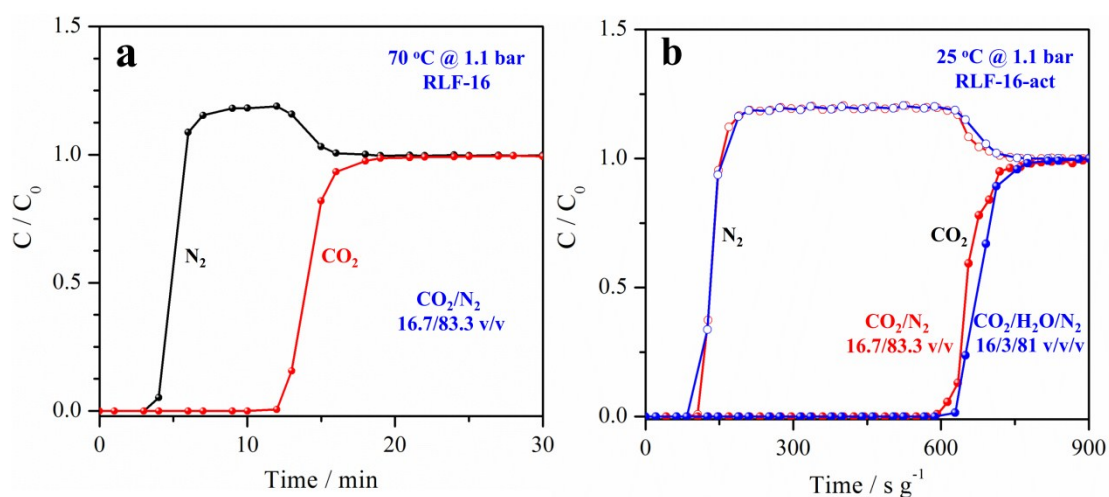


**Figure S6.** (a) Breakthrough curve of RLF-16 for CO<sub>2</sub>/N<sub>2</sub> (16.7/83.3 v/v) mixture at 70 °C and 1.1 bar. (b) Breakthrough curve of RLF-16-act for CO<sub>2</sub>/H<sub>2</sub>O/N<sub>2</sub> (16/3/81 v/v/v) mixture at 25 °C and 1.1 bar.

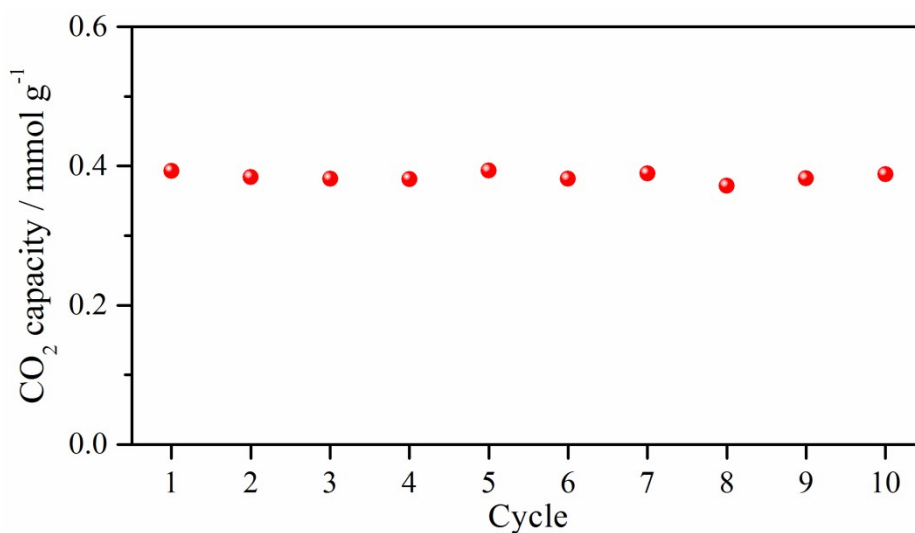


**Figure S7.** Breakthrough measurements: cyclical CO<sub>2</sub> adsorption and desorption of RLF-16-act.

Adsorption condition: CO<sub>2</sub>/N<sub>2</sub> (16.7/83.3 v/v) mixture at 70 °C and 1.1 bar;  
 Desorption condition: Ar (30 mL/min) at 70 °C and 1.1 bar.

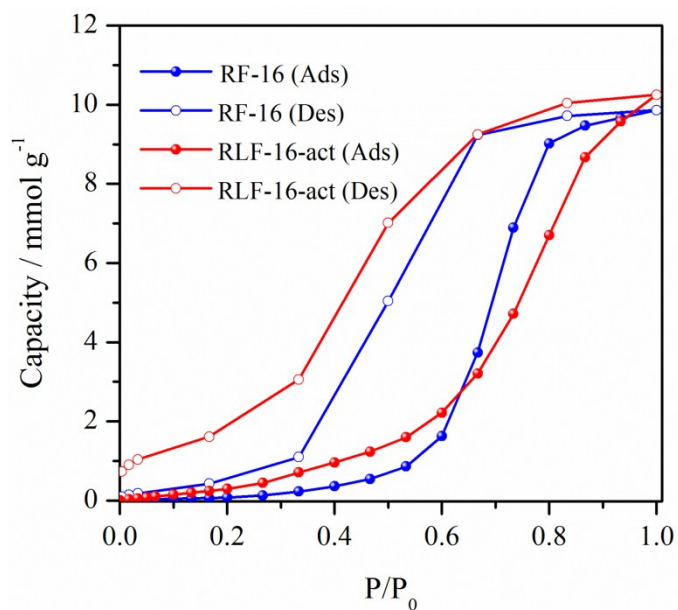


**Figure S8.** H<sub>2</sub>O adsorption (solid symbols) and desorption (empty symbols) isotherm at 25 °C for RLF-16-act and RF-16.

A Hiden IsoChema IGA series microbalance was used to measure the H<sub>2</sub>O adsorption and desorption isotherm in the carbon samples.

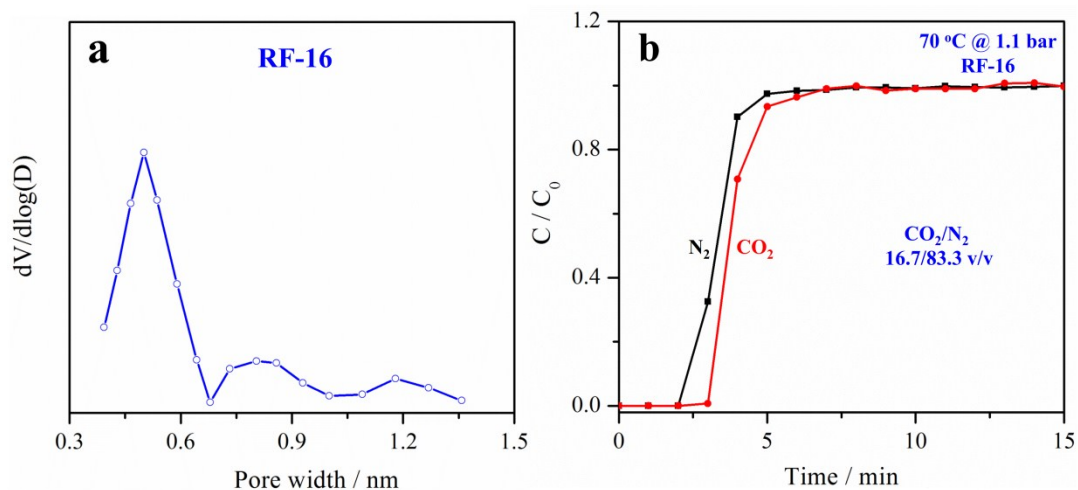


**Figure S9.** (a) Pore size distribution of RF-16. (b) Column breakthrough curve of RF-16 for  $CO_2/N_2$  (16.7/83.3 v/v) mixture at  $70\text{ }^\circ\text{C}$  and 1.1 bar.

**Table S1.** XPS characterization of the obtained porous carbon composites.

Sample	XPS / at.%					
	C	O	Li	Si	Mg	Na
RLF-16	85.46	8.47	2.74	1.68	1.26	0.390
RLF-16-act	86.43	9.37	-	2.50	1.21	0.490

Table S1 Summarizes the chemical compositions of RLF-16 and RLF-16-act characterized by the XPS, and the composition was found to be C, O, Li, Si, Mg and Na.

**Table S2.** CO<sub>2</sub> (1.1 bar and 0.17 bar) and N<sub>2</sub> (1.1 bar) adsorption capacities of the porous carbon composites at different temperature.

Sample		CO <sub>2</sub> capacity / mmol g <sup>-1</sup>					
		0 °C	25 °C	50 °C	70 °C	100 °C	150 °C
RLF-16	1.1 bar	3.8	2.6	2.0	1.5	0.88	0.46
	0.17 bar	1.6	0.97	0.60	0.41	0.18	0.09
RLF-16-act	1.1 bar	4.4	3.0	<b>2.2</b>	<b>1.7</b>	<b>0.98</b>	<b>0.54</b>
	0.17 bar	1.7	1.0	0.62	0.46	0.23	0.12
		N <sub>2</sub> capacity / mmol g <sup>-1</sup>					
RLF-16	1.1 bar	0.66	0.33	0.28	0.17	0.14	0.058
RLF-16-act	1.1 bar	0.80	0.38	0.30	0.23	0.17	0.088

**Table S3.** A comparison table for CO<sub>2</sub> adsorption capacity of reported porous carbons at elevated temperature.

Adsorbent	Precursor	Type	Temp. / °C	P / bar	CO <sub>2</sub> capacity / mmol g <sup>-1</sup>	Source
TEPA-MGC-1	Soybean oil	Mesoporous carbon	75	1	1.3	[S4]
MgOMC-500-16.5	Resols	Mesoporous carbon/MgO	75	1	1.58	[S5]
NPC-S	PAN	Carbon spheres	50	1	2.0	[S6]
om-ph-MR	Resin	Mesoporous polymer	50	1	1.26	[S7]
MOF-177	Zn <sub>4</sub> O(BTB) <sub>2</sub>	MOFs	150	1	0.1	[S8]
γ-Al <sub>2</sub> O <sub>3</sub> NR/RGO/PEI-25	CTAB/GO	Mesoporous composite	75	1	1.14	[S9]
N-enriched carbon (powder)	Soybean	N-enriched carbon	30	0.15	0.93 (CO <sub>2</sub> /N <sub>2</sub> )	[S10]
			75		0.46 (CO <sub>2</sub> /N <sub>2</sub> )	
			120		0.52 (CO <sub>2</sub> /He)	
Mesoporous CN	P123, TMB, TEOS	Carbon nitride spheres	75	1	0.97	[S11]
CP-2-600	Polypyrrole	Porous carbon	25	1	3.9	[S12]
			50		2.1	
			25		2.45	
NMgC-2.4	resorcinol, magnesium nitrate hexahydrate	Carbon composites	75	1	1.17	[S13]
			30		0.792	
MF-700	Melamine-formaldehyde resin	N-enriched carbon	50	1	0.667	[S14]
			75		0.507	
			100		0.354	
			50		0.9	
PEI polymer 4A	PEI Molecular sieve 4A	Polymer Molecular sieve	25	0.02	2.5	
Zr-pillared clay	Zr-pillared clay	Clay	20	1	0.68	[S15]
Basic alumina	Basic alumina	Alumina	20	1	1	
Hydrotalcite	Hydrotalcite	Hydrotalcite	400	0.2	0.5	
MgO	MgO	MgO	400	—	0.2	
<b>RLF-16-act (monolith)</b>	<b>Resin, Laponite</b>	<b>Hierarchical carbon</b>	<b>25</b>	<b>1.1</b>	<b>3.0</b>	<b>Our work</b>
			<b>50</b>		<b>2.2</b>	
			<b>70</b>		<b>1.7</b>	
			<b>100</b>		<b>0.98</b>	
			<b>150</b>		<b>0.54</b>	

**Table S4.** CO<sub>2</sub>/N<sub>2</sub> IAST selectivity of porous carbon composites at 1 bar and different temperature.

Sample	CO <sub>2</sub> /N <sub>2</sub> IAST selectivity (15/85 v/v)					
	0 °C	25 °C	50 °C	70 °C	100 °C	150 °C
RLF-16	34.9	38.3	18.6	18.4	10.1	12.3
RLF-16-act	27.6	33.0	20.1	16.6	9.2	9.5

**Table S5.** Single-site Langmuir-Freundlich adsorption parameters of porous carbon composites at 1 bar.

Sample	Gas	Temp. / °C	$q_{sat}$ / mmol g <sup>-1</sup>	$b$ / bar <sup>-1</sup>	$\nu$	R <sup>2</sup>		
RLF-16	CO <sub>2</sub>	0	7.79696	0.8821	0.68683	0.99985		
		25	5.96786	0.75219	0.77008	0.99995		
		50	6.05084	0.44035	0.8128	0.99997		
		70	4.98831	0.40363	0.86272	0.99998		
		100	5.19751	0.18145	0.89404	0.99998		
		150	31.97025	0.01284	0.92631	0.99976		
	N <sub>2</sub>	0	2.399	0.33739	0.98934	0.99998		
		25	1.06347	0.40045	0.99505	1		
		50	1.55612	0.192	1.00864	0.99996		
		70	1.22541	0.15572	0.999722	0.99993		
		100	0.80518	0.18132	1.08047	0.99923		
		150	0.07713	2.50373	2.28866	0.98768		
		RLF-16-act	CO <sub>2</sub>	0	9.85653	0.72738	0.6918	0.99993
				25	7.72596	0.60378	0.775	0.99996
50	8.46842			0.31762	0.78606	0.99999		
70	6.55663			0.32097	0.83944	0.99998		
100	49.33751			0.01808	0.82822	0.99989		
150	62.21725			0.00779	0.88867	0.99896		
N <sub>2</sub>	0		3.07744	0.30808	1.00777	0.99999		
	25		1.1198	0.45847	1.0106	1		
	50		1.14433	0.30951	1.10245	0.99981		
	70		0.81912	0.35259	1.15446	0.9999		
	100		0.57122	0.38203	1.17321	0.99951		
	150		0.16663	0.92089	1.67163	0.99847		

**Table S6.** Dynamic separation performance of porous carbon composites for CO<sub>2</sub>/N<sub>2</sub> mixture at 1.1 bar.

Sample	Mass / g	CO <sub>2</sub> /N <sub>2</sub> (25 °C)		CO <sub>2</sub> /N <sub>2</sub> (70 °C)	
		CO <sub>2</sub> / mmol g <sup>-1</sup>	Sel.	CO <sub>2</sub> / mmol g <sup>-1</sup>	Sel.
RLF-16	3.078	0.74	+∞	0.35	25
RLF-16-act	2.837	<b>0.90</b>	+∞	<b>0.4</b>	<b>114.3</b>
RLF-16-act (in moisture)	2.863	<b>0.89</b>	+∞	--	

**Calculation of IAST selectivity:**

The uptake isotherm data for guest molecule were fitted with the single-site Langmuir-Freundlich mode:

$$q = q_{sat} \frac{bp^v}{1 + bp^v} \quad (S1)$$

The selectivity for preferential adsorption of CO<sub>2</sub> over component N<sub>2</sub> is defined as

$$S_{CO_2/N_2} = \frac{q_{CO_2}/y_{CO_2}}{q_{N_2}/y_{N_2}} \quad (S2)$$

In equation (S1) and (S2),  $q_{CO_2}$  and  $q_{N_2}$  are the component molar loadings of the adsorbed phase in the mixture, expressed say in the units mmol g<sup>-1</sup>;  $y_{CO_2}$ , and  $y_{N_2} = 1 - y_{CO_2}$ , represent the mole fractions of CO<sub>2</sub> and N<sub>2</sub> in the feed mixture.

### Details of the breakthrough measurements and calculation:

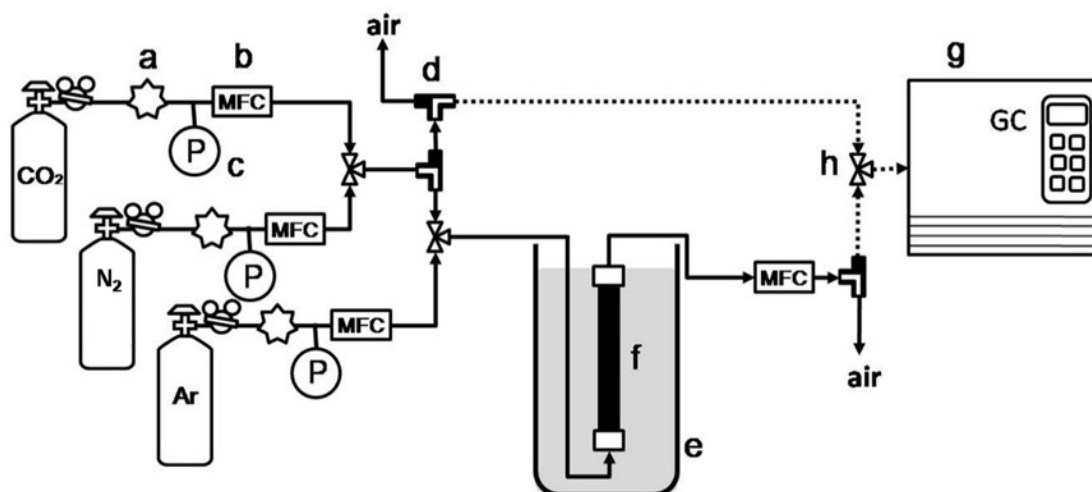


**Figure S10.** Schematic of the gas separation apparatus. (a) pressure controller, (b) mass flow controller, (c) pressure gauge, (d) three-way valves, (e) thermostatic water bath, (f) adsorbent column, (g) gas chromatograph, (h) three-way connection.

The gas mixture was first sent to the gas chromatograph through bypass line and measured its component before the breakthrough measurements. This procedure was necessary to ensure the concentration ratio of gas mixture. Then, the flow of Ar was turned off, and a gas mixture was sent into the sorbent column. The relative amounts of the effluent gases passing through the column were monitored by GC. After the effluent flow rate and the relative amounts of the effluent gases remained unchanged, Ar flow was introduced to activate the adsorbent and then started the next round measurement.

Before the sorbent column, there is a water saturator. To obtain dry isotherms, the water saturator was bypassed. Moisture resistance test was achieved by diverting a

gas mixture to the water saturator. The saturation pressure of H<sub>2</sub>O is 3.1 kPa at 25 °C.

**The capacity and selectivity calculation:<sup>[S16]</sup>**

The adsorption capacity of adsorbent in adsorbent column was calculated from the equation S3:

$$q_i = \frac{C_0 \times t_0 - V_{dead} - \int_0^{t_0} C_i \Delta t}{m} \quad (S3)$$

Where  $q_i$  is the adsorption capacity of the component  $i$ ,  $C_0$  is the total volumetric gas flow rate;  $t_0$  is the adsorption time (min),  $V_{dead}$  is the dead volume of the column and line;  $C_i$  is effluent volumetric flow rate,  $m$  is the mass of adsorbent.

The adsorption selectivity ( $S$ ) was determined from the curves using the following equation:

$$S_{i,j} = \frac{q_i/y_i}{q_j/y_j} \quad (S4)$$

Where  $q$  and  $y$  are the adsorbed amounts and molar fractions in the bulk phase of the components  $i$  and  $j$ , respectively.

## References

- [S4] Y. Wang, X. Bai, F. Wang, H. Qin, C. Yin, S. Kang, X. Li, Y. Zuo and L. Cui, *Sci. Rep.*, 2016, **6**, 26673.
- [S5] Z. Zhang, J. Li, J. Sun, H. Wang, W. Wei and Y. Sun, *Ind. Eng. Chem. Res.*, 2016, **55**, 7880-7887.
- [S6] J. Zhang, R. Yuan, S. Natesakhawat, Z. Wang, Y. Zhao, J. Yan, S. Liu, J. Lee, D. Luo, E. Gottlieb, T. Kowalewski, M. R. Bockstaller and K. Matyjaszewski, *ACS Appl. Mater. Interfaces*, 2017, **9**, 37804-37812.
- [S7] J. H. Lee, H. J. Lee, S. Y. Lim, B. G. Kim and J. W. Choi, *J. Am. Chem. Soc.*, 2015, **137**, 7210-7216.
- [S8] J. A. Mason, K. Sumida, Z. R. Herm, R. Krishna and J. R. Long, *Energy Environ. Sci.*, 2011, **4**, 3030-3040.
- [S9] K. Bhowmik, A. Chakravarty, S. Bysakh and G. De, *Energy Technol.*, 2016, **4**, 1409.
- [S10] J. A. Thote, K. S. Iyer, R. Chatti, N. K. Labhsetwar, R. B. Biniwale and S. S. Rayalu, *Carbon*, 2010, **48**, 396-402.
- [S11] Q. Li, J. Yang, D. Feng, Z. Wu, Q. Wu, S. S. Park, C. S. Ha and D. Zhao, *Nano Res.*, 2010, **3**, 632-642.
- [S12] M. Sevilla, P. Valle-Vigón and A. B. Fuertes, *Adv. Funct. Mater.*, 2011, **21**,

---

2781-2787.

[S13] Z. Zhang, C. Zhu, N. Sun, H. Wang, Z. Tang, W. Wei and Y. Sun, *J. Phys. Chem. C*, 2015, **119**, 9302-9310.

[S14] C. Goel, H. Bhunia and P. K. Bajpai, *J. Environ. Manage.*, 2015, **162**, 20-29.

[S15] X. Xu, C. Song, J. M. Andresen, B. G. Miller and A. W. Scaroni, *Energy Fuels*, 2002, **16**, 1463-1469.

[S16] G. P. Hao, W. C. Li, D. Qian, G. H. Wang, W. P. Zhang, T. Zhang, A. Q. Wang, F. Schüth, H. J. Bongard and A. H. Lu, *J. Am. Chem. Soc.*, 2011, **133**, 11378-11388.